*Antarctic Science 21 (3), 255–267 (2009)* © Antarctic Science Ltd 2009 Printed in the UK doi:10.1017/S0954102009001783

# Noble gas and stable isotope geochemistry of thermal fluids from Deception Island, Antarctica

**MINORU KUSAKABE[1]*, KEISUKE NAGAO[2], TAKESHI OHBA[3], JUNG HUN SEO[4], SUNG-HYUN PARK[1], JONG IK LEE[1] and BYONG-KWON PARK[1]**

[1]*Korea Polar Research Institute, KORDI, Songdo Techno Park, Incheon 406-840, Korea*
[2]*Laboratory for Earthquake Chemistry, University of Tokyo, Tokyo 113-0033, Japan*
[3]*Volcanic Fluid Research Center, Tokyo Institute of Technology, Tokyo 152-8551, Japan*
[4]*School of Earth and Environmental Sciences, Seoul National University, Seoul 151-742, Korea*
**currently at Department of Environmental Biology and Chemistry, University of Toyama, 3190 Gofuku, Toyama 930-8555, Japan*
*kusakabe@sci.u-toyama.ac.jp*

**Abstract:** New stable isotope and noble gas data obtained from fumarolic and bubbling gases and hot spring waters sampled from Deception Island, Antarctica, were analysed to constrain the geochemical features of the island's active hydrothermal system and magmatism in the Bransfield back-arc basin. The $^3He/^4He$ ratios of the gases ($< 9.8 \times 10^{-6}$), which are slightly lower than typical MORB values, suggest that the Deception Island magma was generated in the mantle wedge of a MORB-type source but the signature was influenced by the addition of radiogenic $^4He$ derived from subducted components in the former Phoenix Plate. The $N_2/He$ ratios of fumarolic gas are higher than those of typical mantle-derived gases suggesting that $N_2$ was added during decomposition of sediments in the subducting slab. The $\delta^{13}C$ values of -5 to -6‰ for $CO_2$ also indicate degassing from a MORB-type mantle source. The $H_2/Ar$- and $SiO_2$ geothermometers indicate that the temperatures in the hydrothermal system below Deception Island range from ~150°C to ~300°C. The $\delta D$ and $\delta^{18}O$ values measured from fumarolic gas and hot spring waters do not indicate any contribution of magmatic water to the samples. The major ionic components and $\delta D$-$\delta^{18}O$-$\delta^{34}S$ values indicate that hot spring waters are a mixture of local meteoric water and seawater. Mn and $SiO_2$ in spring waters were enriched relative to seawater reflecting water-rock interaction at depth.

Received 13 June 2008, accepted 9 November 2008

**Key words:** Bransfield back-arc basin, $\delta D$-$\delta^{18}O$-$\delta^{13}C$-$\delta^{34}S$ values, fumarolic gas, $^3He/^4He$ ratio, hot spring water, hydrothermal geochemistry, source mantle

## Introduction

Deception Island (62°43'S, 60°57'W) is the most-westerly subaerial Quaternary active volcano of a series of subaerial and submarine volcanoes situated in Bransfield Basin between the Antarctic Peninsula and the South Shetland Islands (Fig. 1a & b). The recent tectonics of the Bransfield Basin is still controversial. It is currently explained by two different models: 1) the opening of the basin may be related to passive subduction of the former Phoenix Plate and rollback of the South Shetland Trench, or 2) the sinistral movement between the Antarctic and Scotia plates may be causing oblique extension thus generating the Bransfield Basin along the continental margin of Antarctic Peninsula (Maestro *et al.* 2007, and references therein).

There are no systematic changes in lava composition along the central Bransfield Basin. All of the subaerial and submarine lavas show geochemical features indicating a contribution of the subduction components from the former Phoenix Plate (Keller *et al.* 2002). The most MORB-like basalts with the least subduction components occur at both ends of the basin (Fretzdorff *et al.* 2004). It is probable that the mantle was contaminated during subduction of the former Phoenix Plate. The Bransfield Basin is thus thought to be an immature back-arc basin which appears to be at the transition from rifting to spreading. The volcanism there is believed to have occurred at the incipient spreading axis of the basin under extensional tectonics (Keller *et al.* 2002, Lee *et al.* 2008). Submarine hydrothermal activity has also been reported in some of the ridge crests of Bransfield Basin (e.g. Klinkhammer *et al.* 2001).

The rocks of the island are dominated by basalts and basaltic andesites but there is a minor proportion of evolved rocks (Smellie 2001). Deception Island is a horseshoe-shaped flooded caldera which has experienced frequent volcanic eruptions during the 19th century, the last one was in 1970 (Smellie & Lopez-Martinez 2000). There are several subaerial fumaroles and underwater degassing sites in Deception Island (Smellie & Lopez-Martinez 2000, Somoza *et al.* 2004). Hydrothermal activity on the island has been documented by Rey *et al.* (1995) and Somoza *et al.* (2004). Based on a detailed acoustic survey, they revealed three different hydrothermal structures on the Port Foster seafloor; low-mounds, high-mounds and a spire. These structures were produced by

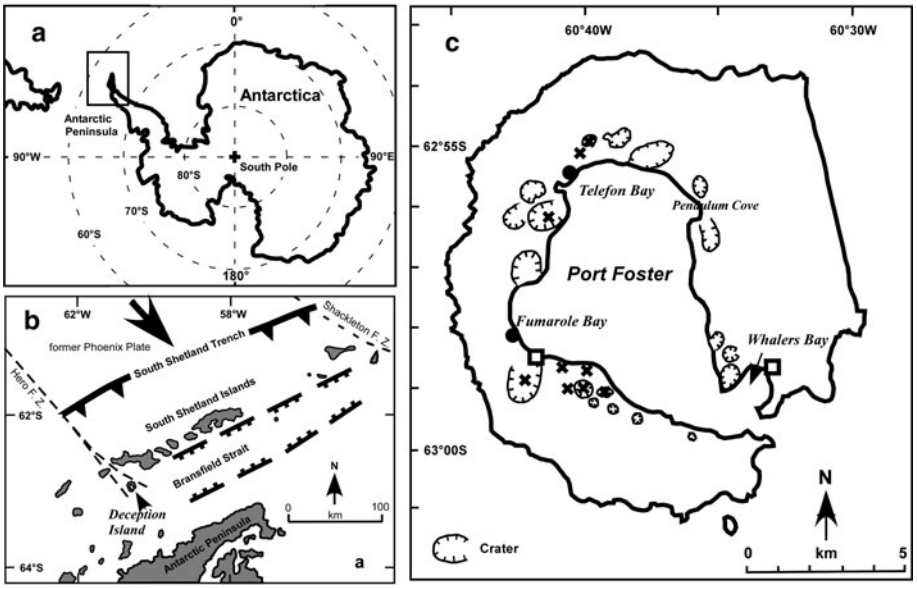


**Fig. 1. a.** A map showing the location of Antarctica. The boxed area is enlarged in **b.** It shows Bransfield Strait which lies between the South Shetland Islands and Antarctic Peninsula (modified from Rey *et al.* 1995). Deception Island is located at the western end of Bransfield Strait. The South Shetland Trench was created by subduction of the former Phoenix plate. **c.** Localities of samples used in this study (map simplified from Smellie & Lopez-Martinez 2000). Fumarolic and bubbling gases were collected from Fumarole Bay and Telefon Bay, respectively, as shown by solid circles. Hot spring waters were collected from Fumarole Bay and Whalers Bay as shown by open squares. Surface waters (crater lake water and glacier meltwater) were collected from the points shown by crosses.

sediment volcanism and seeps driven by high-temperature pore fluids related to the recent volcanic eruption of the island (Somoza *et al.* 2004). From these studies, the Deception Island caldera can be said to be a site of high hydrothermal activity and strong magmatic degassing. In the present study, we report new noble gas and stable isotopic and chemical data obtained following sampling of thermal fluids from Deception Island.

## Samples and analytical methods

Sampling was carried out in December 2006. The fumaroles from Fumarole Bay are currently the most active since the gas temperatures are as high as 97.8°C. The fumarolic gas was collected using a "Giggenbach bottle", an evacuated glass bottle half-filled with concentrated KOH solution. Gases in the headspace of the bottle were analysed with gas chromatography. Chemical species soluble in KOH solution, such as $CO_2$ and $H_2S$, were determined using the wet chemical methods. The fumarolic gas was also collected using a lead-glass bottle with stopcocks at both ends for noble gas analysis. The use of lead-glass bottles prevents diffusive loss of helium during sample storage. We observed very strong gas bubbling at several places around and inside Port Foster, although gas temperature seemed low (atmospheric). We collected such low temperature, bubbling gas from a pond in Telefon Bay using a lead-glass bottle. Air in the bottle was completely replaced by the gas, and was tightly sealed for later laboratory analysis. Hot spring waters were sampled for chemical, stable isotopic and noble gas analyses from steaming ground on the beach of Fumarole Bay and Whalers Bay (Fig. 1b). The samples were collected in a hole of 10–20 cm deep on the beach. A lead-glass bottle was again used for the analysis of dissolved noble gases. Temperatures there were found to be as high as 60°C. We also collected crater lake waters and glacier meltwaters near Fumarole Bay and Telefon Bay to characterize hydrogen and oxygen isotopic features of the surface waters of the island.

The cation composition of hot spring waters was determined with atomic absorption spectrometry for $Na^+$ and $K^+$, and with inductively coupled plasma (ICP) spectrometry for $Mg^{2+}$, $Ca^{2+}$, $Fe^{2+}$ $Mn^{2+}$ and $SiO_2$. The anion composition of hot spring waters was determined with ion chromatography. Carbon isotopic ratios of $CO_2$ from fumarolic and bubbling gases were determined using a stable isotope mass spectrometer. The hydrogen isotopic ratios of waters were analysed with a Zn reduction method,

**Table I.** Chemical and isotopic compositions of fumarolic and bubbling gases from Fumarole Bay and Telefon Bay, Deception Island.

| Sample no. | Sampling locality | Temp. °C | $H_2O$ vol.% | $CO_2$ vol.% | $H_2S$ vol.% | $SO_2$ vol.% | $N_2$ vol.% | $O_2$ vol.% | Ar vol.% | He vol.% | $H_2$ vol.% | $CH_4$ vol.% | $\delta^{34}S$ ‰ | $\delta^{13}C$ ‰ |
|---|---|---|---|---|---|---|---|---|---|---|---|---|---|---|
| DCF-5 | Fumarole Bay | 98.7 | 85.6 | 13.7 | 0.110 | 0.0025 | 0.787 | 0.025 | 0.0038 | 0.0016 | 0.22 | 0.0025 | 0.6 | -5.0 |
| DCF-6 | Fumarole Bay | n.m. | 91.3 | 8.4 | 0.050 | 0.0010 | 0.823 | 0.010 | 0.0043 | 0.0012 | 0.22 | 0.0015 | 0.1 | -5.1 |
| DCF-17 | Telefon Bay | 5 | n.a. | ~100 | n.a. | n.a. | 0.090 | n.a. | 0.0024 | 0.000037 | n.a. | n.a. | n.a. | -6.3 |
| DCF-18 | Telefon Bay | 5 | n.a. | ~100 | n.a. | n.a. | 0.196 | n.a. | 0.0031 | 0.000027 | n.a. | n.a. | n.a. | -6.3 |

n.m. = not measured, n.a. = not analysed

**Table II.** Elemental and isotopic compositions of noble gases of thermal fluids from Deception Island.

a. Elemental composition

| Sample name§ | $^{4}$He ppmV | $^{20}$Ne ppmV | $^{36}$Ar ppmV | $^{40}$Ar ppmV | $^{84}$Kr ppmV | $^{132}$Xe ppmV |
|---|---|---|---|---|---|---|
| FB fumarolic gas (DCF-5) | 16.48 | 0.0125 | 0.110 | 38.0 | 0.00444 | 0.000544 |
| FB fumarolic gas (DCF-6) | 12.12 | 0.0125 | 0.132 | 43.5 | 0.00586 | 0.000730 |
| TB bubbling gas (DCF-17) | 0.368 | 0.0036 | 0.078 | 23.6 | 0.00507 | 0.000746 |
| TB bubbling gas (DCF-18) | 0.272 | 0.0085 | 0.103 | 31.0 | 0.00529 | 0.000675 |
| FB hot spring water (DCF-22) | 3.35E-07# | 1.01E-08# | 1.97E-7# | 5.89E-5# | 7.88E-09# | 7.09E-10# |
| Air (ppmV)* | 5.24 | 16.5 | 31.5 | 9300 | 0.649 | 0.0234 |
| Air dissolved in water at 0°C** (cc/g) | 4.90E-08 | 2.04E-07 | 1.67E-06 | 4.96E-04 | 7.06E-08 | 5.21 E-09 |

b. Isotopic ratios of He, Ne and Ar

| Sample name | $^{3}$He/$^{4}$He E-6 | $^{20}$Ne/$^{22}$Ne | $^{21}$Ne/$^{22}$Ne | $^{38}$Ar/$^{36}$Ar | $^{40}$Ar/$^{36}$Ar | $^{40}$Ar/$^{4}$He | $^{4}$He/$^{20}$Ne |
|---|---|---|---|---|---|---|---|
| FB fumarolic gas (DCF-5) | 9.78(14) | 9.808 (48) | 0.02947 (20) | 0.1879(6) | 346.57 (44) | 2.31 | 1320 |
| FB fumarolic gas (DCF-6) | 9.37(13) | 9.706 (46) | 0.02859 (42) | 0.1877(4) | 329.57 (46) | 3.59 | 971 |
| TB bubbling gas (DCF-17) | 9.75(15) | 9.491 (35) | 0.02808 (23) | 0.1883(6) | 303.14(42) | 64.2 | 102 |
| TB bubbling gas (DCF-18) | 9.43(13) | 9.596 (36) | 0.02857 (26) | 0.1881 (4) | 300.46 (33) | 114 | 32.0 |
| FB hot spring water (DCF-22) | 9.57(13) | 9.757(31) | 0.02891 (17) | 0.1888(4) | 298.70(61) | 176 | 331.1 |
| Air* | 1.4 | 9.80 | 0.0290 | 0.188 | 296.0 | 1780 | 0.318 |

c. Isotopic ratios of Xe relative to $^{132}$ Xe

| Sample name | $^{124}$Xe | $^{126}$Xe | $^{128}$Xe | $^{129}$Xe | $^{130}$Xe | $^{131}$Xe | $^{132}$Xe | $^{134}$Xe | $^{136}$Xe |
|---|---|---|---|---|---|---|---|---|---|
| FB fumarolic gas (DCF-5) | 0.00355 (20) | 0.00338 (19) | 0.0716 (14) | 0.9840 (62) | 0.1520 (13) | 0.7894 (86) | 1 | 0.3891 (44) | 0.3299 (31) |
| FB fumarolic gas (DCF-6) | 0.00344 (18) | 0.00330 (20) | 0.0713 (11) | 0.9835 (31) | 0.1511 (12) | 0.7869 (61) | 1 | 0.3873 (45) | 0.3300 (29) |
| TB bubbling gas (DCF-17) | 0.00345 (21) | 0.00335 (17) | 0.0716 (10) | 0.9891 (31) | 0.1515 (18) | 0.7896 (67) | 1 | 0.3889 (42) | 0.3314 (29) |
| TB bubbling gas (DCF-18) | 0.00353 (18) | 0.00334 (18) | 0.0713 (10) | 0.9806 (44) | 0.1518 (11) | 0.7875 (54) | 1 | 0.3901 (40) | 0.3317 (27) |
| FB hot spring water (DCF-22) | 0.00334 (20) | 0.00344 (22) | 0.0712 (9) | 0.9813 (38) | 0.1513 (11) | 0.7864 (60) | 1 | 0.3867 (43) | 0.3301 (24) |

§FB = Fumarole Bay, TB = Telefon Bay.

#Concentrations in water are given in cc/g water.

*Ozima & Podosek 2002.

**Kipfer *et al.* 2002.

Note: Number in parenthesis denotes the analytical error (1σ) corresponding to the last digit(s) of each analysis.

while oxygen ratios were analysed using an automated $H_2O$–$CO_2$ exchange method. The sulphur isotopic ratio of $SO_4^{2-}$ dissolved in the hot spring waters was also analysed using $SO_2$ as an analytical gas. Stable isotopic ratios are expressed in a conventional δ-notation using VSMOW, VPDB and Canyon Diablo troilite as the standard materials for hydrogen, oxygen, carbon and sulphur isotopic ratios respectively. Noble gas elemental and isotopic compositions were determined for fumarolic gases, bubbling gases and hot spring water. Noble gases were measured with a modified VG5400 (MS-III) mass spectrometer at the University of Tokyo.

## Results

Table I shows the chemical analysis of fumarolic gas from Fumarole Bay and bubbling gas from Telefon Bay. The rate of fumarolic gas emission was highest at high tides. Hence the gas concentrations varied due to addition evaporating seawater at the time of sample collection. If $H_2O$ is excluded, then the most abundant gaseous components were $CO_2$ (8∼14 vol.%) followed by $N_2$ (∼0.8 vol.%) and $H_2S$ (0.05∼0.11 vol.%). $SO_2$ was found at only very low concentrations, i.e. 0.0010∼0.0025 vol.%. The content of $O_2$ was generally low (< 0.025 vol.%), indicating that contamination by air during sampling was small. Our gas analysis is consistent with high concentrations of $CO_2$ (75∼90 vol.%) and $H_2S$ (0.3∼0.9 vol.%) reported by Valentin *et al.* (1989) (cited in Somoza *et al.* 2004), but their values cannot be directly compared with ours because they did not report $H_2O$ concentration. Of the minor components, $H_2$ and He concentrations were 0.22 vol.% and from 12 to 16 ppmv, respectively. Ortiz *et al.* (1987) (cited in Rey *et al.* 1995) reported wider concentration ranges of these gases, i.e. 100∼660 ppmv for $H_2$ and 10∼190 ppmv for He. The bubbling gas from Telefon Bay consisted mostly of $CO_2$ with minor concentrations of the other gases, although we did not analyse components other than $N_2$, Ar and He. Concentrations of these gases were very low, indicating air contamination during sampling was kept to a minimum.

The following results are the first detailed noble gas analyses for hydrothermal fluids obtained from Deception Island. Elemental and isotopic analyses of noble gases are given in Table II as a) elemental composition of He, Ne, Ar, Kr and Xe, b) isotopic ratios of He, Ne and Ar, and c) isotopic composition of Xe. Analytical accuracies of elemental concentrations are about 10%, and analytical errors of isotopic ratios are given in 1σ. Helium isotopic ratios are close to but slightly lower those of the MORB-type He, suggesting predominant contribution of He of mantle origin. Neon isotopic ratios of gas and water samples from Fumarole Bay (DCF-5, DCF-6 and DCF-22 (see Table II for sample names.)) are atmospheric. Gas samples DCF-17 and DCF-18 from Telefon Bay, however,

**Table III.** Chemical and isotopic compositions of hot spring waters from Fumarole Bay and Whalers Bay, Deception Island.

| Sample | Sampling locality | Temp. °C | pH | Na (ppm) | K (ppm) | Mg (ppm) | Ca (ppm) | Mn (ppm) | $SiO_2$ (ppm) | cr (ppm) | $SO_{4}$- (ppm) | δD (‰) | $\delta^{18}O$ (‰) | $\delta^{34}S$ (‰) |
|---|---|---|---|---|---|---|---|---|---|---|---|---|---|---|
| DCF-7 | Fumarole Bay #1 | 53.7 | 7.53 | 5583 | 262 | 801 | 495 | 2.94 | 115.9 | 12980 | 1744 | -21.2 | -2.75 | |
| DCF-20 | Fumarole Bay #2 | 50.7 | 7.84 | 7008 | 303 | 835 | 495 | 2.39 | 147.1 | 17740 | 2496 | -20.8 | -2.87 | 19.4 |
| DCF-16 | Whalers Bay | 57.5 | 7.64 | 5673 | 257 | 1116 | 461 | 1.16 | 114.9 | 13160 | 1796 | -8.3 | -0.73 | 20.2 |
| Seawater* | | | | 10800 | 399 | 1290 | 412 | 2.0E-4 | 4.0** | 19400 | 2770 | 0.0 | 0.00 | 20.5 |

*CRC Handbook of Chemistry and Physics, 74th Edition (Lide 1993–1994).
**Estimated from Hydrographic Atlas of the World Ocean Circulation Experiment (WOCE) (Orsi & Whitworth 2005).

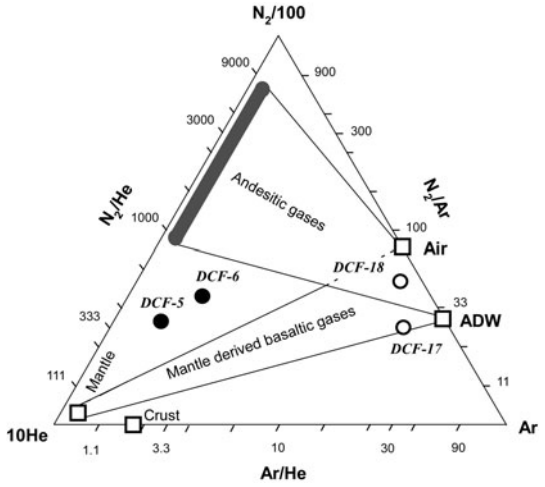


**Fig. 2.** Relative $N_2$-He-Ar composition of gases from Fumarole Bay (DCF-5 and DCF-6) and Telefon Bay (DCF-17 and DCF-18). Refer to Giggenbach (1997) for the areas for the mantle derived basaltic gases and andesitic gases.

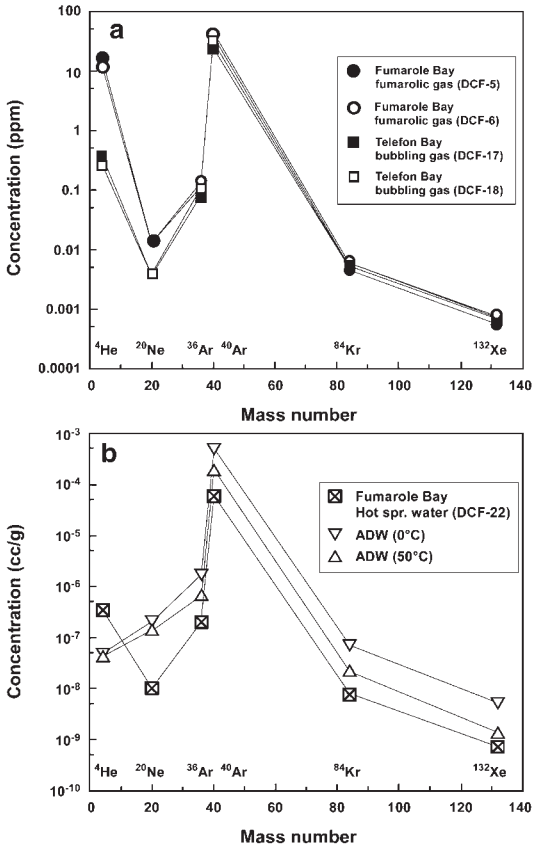


**Fig. 3. a.** Abundance pattern of noble gases in the Fumarole Bay fumarolic gases (DCF-5 and DCF-6) and Telefon Bay bubbling gases (DCF-17 and DCF-18). **b.** Abundance pattern of noble gases dissolved in the Fumarole Bay hot spring water (DCF-22), and in water saturated by air (ADW) at 0°and 50°C (Kipfer *et al.* 2002).

show $^{20}Ne/^{22}Ne$ and $^{21}Ne/^{22}Ne$ ratios slightly lower than the atmospheric values by $3.2 \pm 0.8\%$ ($2\sigma$) and $3.2 \pm 1.6\%$ ($2\sigma$) for DCF-17, and $2.1 \pm 0.8\%$ ($2\sigma$) and $1.5 \pm 0.8\%$ ($2\sigma$) for DCF-18. The low values may have been caused by mass fractionation that favours enrichment in heavier isotopes during transport of Ne from atmosphere to the bubbling gases. $^{38}Ar/^{36}Ar$ and Xe isotopic ratios agree with the atmospheric values. Small enrichment in $^{40}Ar$ is observed in all the gas samples, which indicates contribution of Ar with high $^{40}Ar/^{36}Ar$ from mantle or crustal rocks beneath the island.

Chemical analyses of hot spring waters from Fumarole Bay and Whalers Bay are shown in Table III. The seawater contribution to these hot spring waters is high as exemplified by high concentrations of major cations and anions, i.e. $Na^+$, $K^+$, $Ca^{2+}$, $Mg^{2+}$, $Cl^-$ and $SO_4^{2-}$, and by hydrogen, oxygen and sulphur isotopic ratios. However, Mn was highly enriched compared with seawater. Significant enrichment of $SiO_2$ was also observed. Our observations suggest that these components were extracted from underlying volcanic rocks during water-rock interaction.

## Discussion

### *Source of volatiles*

Relative abundance of $N_2$, He and Ar

The relative abundance of $N_2$, He and Ar of volcanic and geothermal gases has been used to classify their sources (Giggenbach 1997). These abundances have been calculated for Deception Island gases from the data in Table I and plotted in Fig. 2. Fumarolic gases from Fumarole Bay (DCF-5 and DCF-6) plot above a triangular area for mantle derived basaltic gases mixed with air or air dissolved in water (ADW). Bubbling gases from Telefon Bay (DCF-17 and DCF-18) plot close to air and ADW, indicating a large contribution of atmospheric components, although the atmospheric contamination of He to the observed He is less than 1% for these samples. Figure 2 suggests that the Fumarole Bay fumarolic gases are mixtures of mantle derived basaltic gases and gases from arc-type magma which are believed to be relatively enriched in $N_2$. Enrichment of $N_2$ in andesitic gases may be due to the contribution of nitrogen from sediments carried by a subducting slab beneath the arc systems (Matsuo *et al.* 1978, Kita *et al.* 1993). Thus the mantle beneath the Bransfield basin is suggested to contain some subducted components from the former Phoenix Plate.

Elemental abundance of noble gases

The concentrations of noble gases in Fumarole Bay gas samples (DCF-5 and DCF-6) and in Telefon Bay gas samples (DCF-17 and DCF-18) in Table II are plotted in Fig. 3a. The concentrations of Ar, Kr and Xe of the four gas samples are

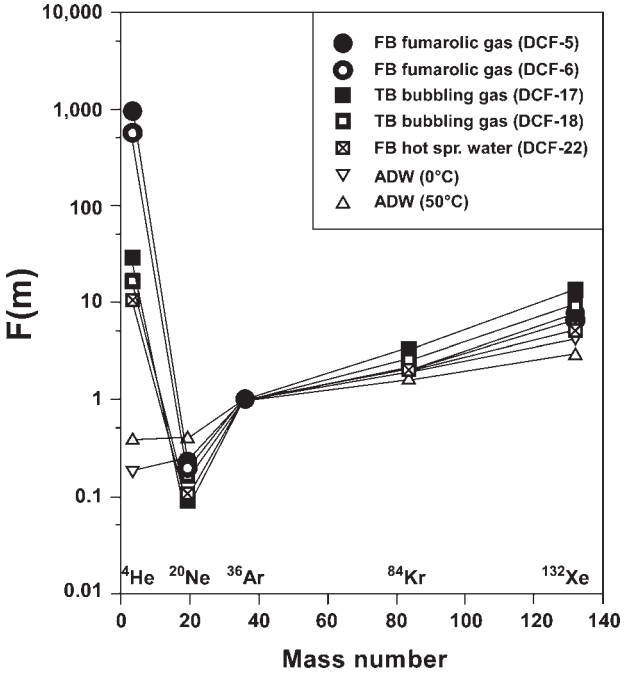


**Fig. 4.** Noble gas abundance patterns of the fumarolic and bubbling gases from Deception Island relative to air composition. The relative abundance is expressed in terms of F(m) defined as $F(m) = ({}^{m}X/{}^{36}Ar)_{sample}/({}^{m}X/{}^{36}Ar)_{air}$, where $^{m}X$ stands for $^{4}He$, $^{20}Ne$, $^{36}Ar$, $^{84}Kr$ or $^{132}Xe$. FB and TB refer to Fumarole Bay and Telefon Bay, respectively.

almost identical, whereas He and Ne concentrations of gases from Fumarolic Bay are significantly higher than those of the Telefon Bay gases. This suggests that magmatic He appears to be more effectively transported to the surface in the Fumarole Bay area compared to the Telefon Bay area. The concentrations of noble gases in the Fumarole Bay hot spring water (DCF-22) are plotted in Fig. 3b along with those for air dissolved in pure water (ADW) at 0° and 50°C for comparison. Concentrations of all noble gases except for He in the water sample are clearly lower than those saturated in water. The $^{20}Ne$, $^{36}Ar$, $^{84}Kr$ and $^{132}Xe$ concentrations in the DCF-22 water sample are lower than those in ADW at 50°C by factors 0.07, 0.31, 0.37, 0.52, respectively. The low concentrations may have resulted from partial removal of heavy noble gases from water phase when it vaporized, because noble gases tend to be preferentially partitioned into vapour phase (e.g. Ballentine *et al.* 2002 and references therein).

The higher concentration of He compared to the ADW may be due to a high supply of mantle He in the source region of the Fumarole Bay hydrothermal system. Relative elemental abundance patterns of the noble gases, normalized to air composition, are shown in Fig. 4 as a function of F(m). F(m) is defined as $({}^{m}X/{}^{36}Ar)_{sample}/({}^{m}X/{}^{36}Ar)_{air}$, where $^{m}X$ stands for $^{4}He$, $^{20}Ne$, $^{36}Ar$, $^{84}Kr$ or $^{132}Xe$ (Ozima & Alexander 1976). The abundance patterns of ADW at 0°C and 50°C (Kipfer *et al.* 2002) are also shown for comparison. The general features of Fig. 4 are: 1) thermal fluids from Deception Island are all enriched in He compared to ADW. Fumarolic gas is most enriched in He compared to ADW by approximately three orders of magnitude, bubbling gas by 20∼30 times more than ADW, and gas dissolved in hot spring water by ∼10 times more than ADW, 2) the thermal fluids from Deception Island are depleted in Ne relative to ADW, and 3) a significant enrichment of Xe compared to ADW is seen. Enrichment of He suggests the presence of He derived from magma, as supported by high $^{3}He/^{4}He$ ratios as will be discussed later. Other noble gases were probably derived from the atmosphere through groundwater and/or seawater, although a small contribution of radiogenic $^{40}Ar$ from magma is recognizable as mentioned above. Depletion of Ne and enrichment of Kr and Xe relative to ADW may have resulted from elemental fractionation. The progressive enrichment in heavier noble gases may indicate the contribution from recycled noble gases trapped in subducted sediments (e.g. Fukumoto *et al.* 1986, Ozima & Podosek 2002). This is consistent with the $N_2$ enrichment shown in Fig. 2.

### $^{3}He/^{4}He$ ratio

The $^{3}He/^{4}He$ values in deep seawater of the Bransfield Strait have been found to exceed the atmospheric value by up to ∼7% (Schlosser *et al.* 1988). Schlosser *et al.* interpreted this excess to result from addition of $^{3}He$ into the deep waters of the Bransfield Strait. The estimated $^{3}He/^{4}He$ ratio of the added helium of $2.4\text{-}5.0 \times 10^{-6}$ is lower than the ratio of mantle helium. Schlosser *et al.* suggested that the added helium contains radiogenic component from continental crust underlying the Bransfield Strait. In Deception Island, recent measurement of $^{3}He/^{4}He$ ratios in the Port Foster seawater clearly indicates an injection of deep magmatic helium (Park *et al.* 2007). The Port Foster deep water at ∼135 m has $^{3}He/^{4}He$ values as high as $3.5 \times 10^{-6}$, 2.5 times higher than atmospheric. Park *et al.* (2007) discussed that the high $^{3}He/^{4}He$ ratio could be attributed to the venting of hot (> 200°C) hydrothermal fluids from the sea floor. Since hydrothermal activity is ubiquitous in and around Port Foster, we expect to find magmatic He uncontaminated by He dissolved in seawater in fumarolic gases. This may represent the end member He of the hydrothermal fluids discharging from the sea floor.

The $^{3}He/^{4}He$ ratios from thermal fluids from Deception Island listed in Table IIb show consistently high values of $9.37 \times 10^{-6}$ to $9.78 \times 10^{-6}$, whereas the $^{20}Ne/^{22}Ne$, $^{21}Ne/^{22}Ne$ and $^{38}Ar/^{36}Ar$ ratios are very close to atmospheric values. The $^{40}Ar/^{36}Ar$ ratios are only slightly higher than atmospheric, implying addition of a minute amount of magmatic Ar. The high $^{3}He/^{4}He$ ratios suggest that the thermal fluids from Deception Island contain He of magmatic origin. The $^{4}He/^{20}Ne$ ratios are considered a

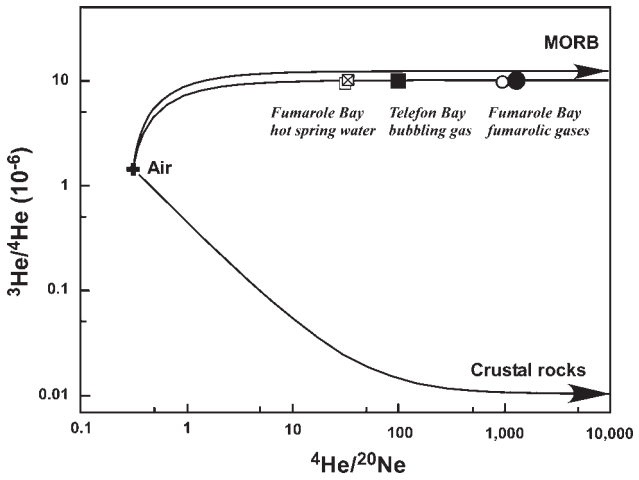


**Fig. 5.** $^3He/^4He$ vs. $^4He/^{20}Ne$ plot of the Fumarole Bay fumarolic gases (DCF-5 and DCF-6), Telefon Bay bubbling gases (DCF-17 and DCF-18) and gases dissolved in the Fumarole Bay hot spring water (DCF-22). Mixing curves between air and gases directly derived from MORB-source mantle ($^3He/^4He = 11.5 \times 10^{-6}$) and between air and crustal rocks ($^3He/^4He = 0.01 \times 10^{-6}$) are shown. See text for the end-member compositions. The Deception Island gases plot slightly below the MORB-Air mixing curve with the end-member $^3He/^4He$ ratio of $9.8 \times 10^{-6}$.

good indicator of atmospheric contamination (Torgersen & Jenkins 1982). The highest observed $^4He/^{20}Ne$ ratio of fumarolic gas from Fumarole Bay (DCF-5) was 1320, and about 4000 times higher than the atmospheric $^4He/^{20}Ne$ ratio of 0.32 (Table IIb). The $^4He/^{20}Ne$ ratios of bubbling gas from Telefon Bay (DCF-17) and from Fumarole Bay hot spring water (DCF-22) were 102 and 33, respectively. These values are 320 to 100 times higher than the atmospheric $^4He/^{20}Ne$ ratio. These observations suggest that these gases derive from magma, since magmatic gases are characterized by high $^4He/^{20}Ne$ ratios. In Fig. 5, the $^3He/^4He$ ratios are plotted against $^4He/^{20}Ne$ ratios for the samples under consideration. The mixing curves in Fig. 5 were drawn assuming that the atmospheric component of $^3He/^4He$ is $1.4 \times 10^{-6}$ and $^4He/^{20}Ne$ is 0.32, the MORB source mantle component is $11.5 \times 10^{-6}$ and $^4He/^{20}Ne$ is 40 000 (Aka *et al.* 2001), and the crustal radiogenic component of $^3He/^4He$ is $1.0 \times 10^{-8}$ and $^4He/^{20}Ne$ is 100 000 (Ballentine & Burnard 2002). In the $^3He/^4He$-$^4He/^{20}Ne$ space (Fig. 5), the Deception Island fluids plot slightly below the MORB-atmosphere mixing line and lie nicely on a mixing curve between a magmatic component end-member characterized by a high $^3He/^4He$ of $\sim 9.8 \times 10^{-6}$ and $^4He/^{20}Ne$ ratio greater than 1000, and the atmospheric end-member. The $^3He/^4He$ ratios of $\sim 9.8 \times 10^{-6}$ for Deception Island are slightly lower than those of MORB glasses from various areas (e.g. Graham 2002). Our preliminary $^3He/^4He$ analysis of gas extracted from rocks and minerals from the island is consistent with the above gas values in that the rock data never exceed $10 \times 10^{-6}$ (K. Nagao, personal communication 2008)

The MORB values are known to be homogeneous; $11.3 \times 10^{-6}$ for Atlantic MORB, $11.4 \times 10^{-6}$ for Pacific MORB, and $11.5 \times 10^{-6}$ for Indian MORB (median values, Graham 2002). However, the $^3He/^4He$ ratios of back-arc basin volcanic rocks are highly variable. Although the mean data is close to the MORB values, the individual values are highly variable even in a given back-arc basin (Hilton *et al.* 2002). For example, the highest value of $30.9 \times 10^{-6}$

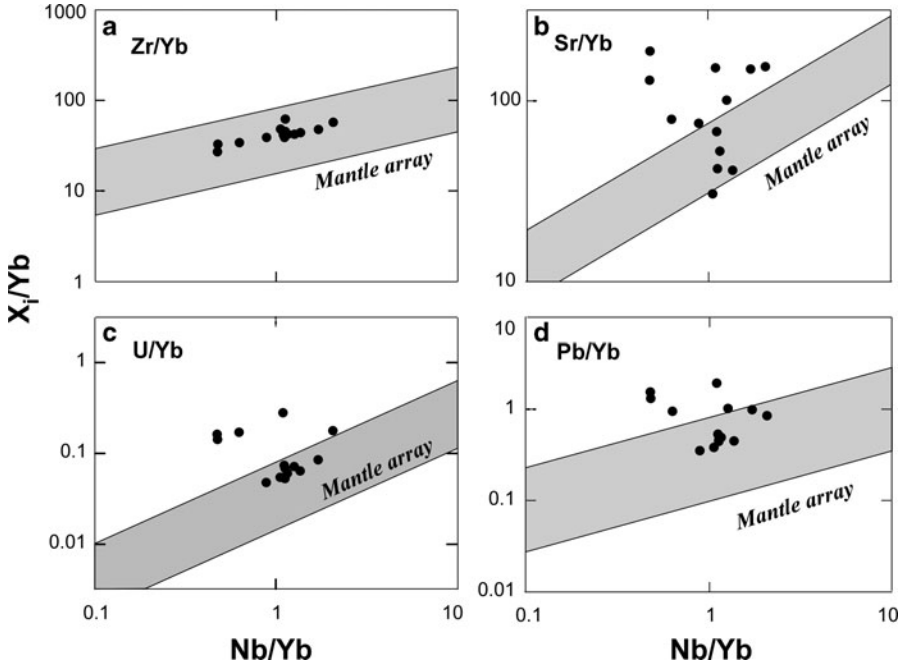


**Fig. 6.** Incompatible element ratios for volcanic rocks of the Bransfield Strait back-arc basin. **a.** Zr/Yb-Nb/Yb, **b.** Sr/Yb-Nb/Yb, **c.** U/Yb-Nb/Yb, and **d.** Pb/Yb-Nb/Yb. Data were taken from Keller *et al.* (2002). The shaded area indicates the range of incompatible element ratios in MORB from the fossilized spreading centre of the Antarctic-Phoenix Ridge (Choe *et al.* 2007).

and the lowest value of $1.2 \times 10^{-6}$ were documented at Lau Basin (Poreda & Craig 1992). A large variation was also found at Manus Basin (Macpherson *et al.* 1998). The high values have been interpreted to be related to the nearby hotspots. The $^3He/^4He$ ratios of back-arc basin volcanics that are lower than those of MORB may result from the situations where 1) the mantle wedge is depleted in helium, so radiogenic helium is accentuated, 2) the mantle wedge is enriched in U and Th derived from the subducted slab, 3) the magmas acquired crustal radiogenic helium during storage and/or ascent (Hilton *et al.* 2002), or 4) the mantle wedge contains enriched components related to a mantle plume. It is difficult to constrain the geochemical features of the mantle beneath the Bransfield back-arc basin on the basis of He isotopic variations alone. The geochemical characteristics of the mantle beneath Bransfield basin may be estimated from the analysis of trace element geochemistry of volcanic rocks collected from the area. High field strength elements such as Zr, Nb and Yb have been considered good geochemical indicators to characterize the slab influence on the wedge mantle, because they have low mobility in fluids and low concentration in sediments. We followed the approach of Pearce *et al.* (1995) which has been applied to estimate the subduction input to the wedge mantle beneath the South Shetland Islands by Lee *et al.* (2008). In Fig. 6 we plot $X_i/Yb$ against Nb/Yb where $X_i$ denotes an incompatible element under consideration. Since neither Nb nor Yb are mobile during fluid formation from the subducting slab, any increment of the $X_i/Yb$ ratio relative to mantle-derived oceanic basalts or "mantle array" could be interpreted to indicate the addition of $X_i$ from the slab to the wedge mantle. The trace element data of volcanic rocks collected from the Bransfield back-arc basin have been obtained by Keller *et al.* (2002) and used for the construction of Fig. 6. The data for the mantle array which represents the trace element composition of MORB samples from the fossilized spreading centre of the Antarctic-Phoenix Ridge are from Choe *et al.* (2007). As seen in Fig. 6a, the Zr/Yb ratios plot in the mantle array as expected, suggesting that Zr and Yb are immobile and the abundance of Zr and Yb in the slab is low. On the other hand, approximately half of Sr/Yb, U/Yb and Pb/Yb ratios plot above the mantle array (Fig. 6b–d). Although it is not included in Fig. 6, the Th/Yb ratios plot is similar to the Sr/Yb, U/Yb and Pb/Yb ratios. Since Sr and Pb will be strongly partitioned into fluids relative to crystalline phases, it is conceivable that the above-mentioned elements (Sr, Pb, U and Th) contaminated the wedge mantle beneath the Bransfield basin in the form of fluid derived from the slab that carried altered oceanic crust or sediments. This interpretation is consistent with the geochemistry of Bransfield back-arc volcanics (Keller *et al.* 2002). Keller *et al.* suggested that rocks from the south-west end of the Bransfield rift are almost MORB-like but enriched in Cs and Pb. The Pb enrichment was interpreted to have been derived from metalliferous sediments and fluids from a subducting slab underneath the Bransfield basin. A similar interpretation has been given to the trace element geochemistry of arc volcanics from South Shetland Islands (Kraus 2005, Lee *et al.* 2008). These observations are consistent with $N_2/He$ ratios of Fumarole Bay fumarolic gas that are higher than those of typical mantle-derived basaltic gases (Fig. 2). From the above discussion, we believe that the end member helium with the $^3He/^4He$ value of $\sim 9.8 \times 10^{-6}$ from the Deception Island hydrothermal fluids has been derived from magma generated in a mantle wedge that was influenced by subducted components from the former Phoenix Plate.

Carbon dioxide in the fumarolic and bubbling gases from Deception Island has a limited range of $\delta^{13}C$ values of -6.3 to -5.0 ‰ (Table I). These values are typical for mantle carbon (e.g. Taylor 1986) and indicate that $CO_2$ is also of mantle origin and that the $CO_2$ contribution from sedimentary and limestone sources is small. $CO_2/^3He$ ratios coupled with $\delta^{13}C$ values have been used as an indicator to constrain the source of $CO_2$ and He in volcanic fluids (e.g. Marty & Jambon 1987). Based on the $CO_2/^3He$ versus $\delta^{13}C$ relationship Sano & Marty (1995) evaluated the relative proportion of carbon sources in volcanic and hydrothermal fluids from subduction zones under the assumptions that the carbon sources were MORB-source mantle, marine carbonate and sedimentary organic materials in subducting slab. The end-member values used for the estimation are $CO_2/^3He = 1.5 \times 10^9$ and $\delta^{13}C = -6.5$ ‰ for the MORB-source mantle, $CO_2/^3He = 1 \times 10^{13}$ and $\delta^{13}C = 0$ ‰ for the marine carbonate, and $CO_2/^3He = 1 \times 10^{13}$ and $\delta^{13}C = -30$ ‰ for the sedimentary carbon. In the case of Japanese volcanic gases the major carbon contributor was subducted marine carbonate and the mantle source was up to 20% (Sano & Marty 1995). A similar conclusion has been obtained for the Lesser Antilles island arc geothermal fluids (van Soest *et al.* 1998). Basalts and hydrothermal fluids from back-arc basins such as Lau Basin (Hilton *et al.* 1993), Mid-Okinawa Trough (Ishibashi *et al.* 1995), North Fiji Basin (Nishio *et al.* 1998) and Manus Basin (Shaw *et al.* 2004) were also studied using the same geochemical parameters. These studies showed a wide range of $^3He/^4He$ and $C/^3He$ ratios and indicate that mantle beneath the basins are affected by degassing and contamination of crustal carbon. The $CO_2/^3He$ ratios of the Fumarole Bay fumarolic gases calculated from the data in Tables I & II are $0.7 \sim 0.9 \times 10^9$. These are slightly lower than the mean depleted mantle values of $\sim 2 \times 10^9$. The reason why the Deception Island gases have $CO_2/^3He$ ratios lower than those of MORB may be because part of $CO_2$ has been fixed as carbonate through the water-rock interaction, e.g.

$$3\ \text{K-feldspar} + CO_2 + Ca^{2+} = \text{K-mica} + \text{calcite} + 2K^+,$$

in the deep hydrothermal system (Giggenbach 1991). Since the carbon isotopic fractionation factor between calcite and $CO_2$ is small at hydrothermal temperatures (-3‰ at 300°C and +1‰ at 150°C, Chako *et al.* 2001), $\delta^{13}C$ values at source would not be significantly influenced by the mineral control. Although the number of $^3He/^4He$ and $CO_2/^3He$ ratios and $\delta^{13}C$ values of the Deception Island gases is limited, they indicate that the majority of He and $CO_2$ is likely to have derived from the MORB-like source mantle that was influenced by fluids from the slab as discussed above.

*Subsurface hydrothermal system*

Subsurface temperature

Hydrothermal manifestations such as fumaroles, steaming grounds, and hot springs along the beaches of Deception Island indicate the existence of a hydrothermal system beneath the island. Seismic and geochemical studies by Rey *et al.* 1995 and Somoza *et al.* 2004 also indicate hydrothermal activity on the island. Valentin *et al.* (1989) (cited in Somoza *et al.* 2004) suggested on the basis of gas chemistry that the temperature of the hydrothermal system is about 219°C. We estimated the temperature of the hydrothermal system using a hydrogen geothermometer. This was originally proposed by Taran (1986) and later revised by Giggenbach (1991). He introduced a $H_2/Ar$ ratio into the geothermometer and assumed that $H_2$ and Ar behave together. The $H_2/Ar$ ratio is used to minimize the effect on the geothermometer of preferential loss or addition of hydrogen after its separation from liquid phase. The fugacity ratio of $H_2/H_2O$ in hydrothermal systems is governed by redox equilibria of Fe(II) and Fe(III) in rocks hosting a hydrothermal system, and is practically constant over a wide range of temperature (Giggenbach 1987). The hydrogen geothermometer essentially utilizes the temperature dependence of the hydrogen distribution coefficient between gas phase and liquid phase. The assumptions are that i) the hydrothermal reservoir consists of a liquid phase only, ii) the redox equilibrium between Fe(II) and Fe(III) in host rocks has been established, iii) a tiny fraction of vapour phase leaks out of the hydrothermal system to the surface without disturbing $H_2/H_2O$ ratio of the system, and iv) Ar derives from air dissolved in groundwater. Accepting these assumptions, the observed vapour-phase $H_2/Ar$ ratio was used for calculations. Equation of the $H_2/Ar$ geothermometer is;

$$t_{H2/Ar} = 71.3 \times (2.505 + \log(X_{H2}/X_{Ar})),$$

where $X_{H2}$ and $X_{Ar}$ denote mole fraction of hydrogen and argon in the gas analysed and $t_{H2/Ar}$ is in °C. The $H_2$ and Ar data for Fumarole Bay fumarolic gases shown in Table I gave temperatures around 300°C for the underlying hydrothermal system. Similar temperatures were calculated for bubbling gases collected at Telefon Bay using a $CO_2$/Ar geothermometer (Giggenbach 1991). The equation of the $CO_2$/Ar geothermometer is:

$$\log(X_{CO2}/X_{Ar}) = 0.0277^{*}t_{CO2/Ar}\text{-}7.53 + 2048/(t_{CO2/Ar} + 273),$$

where $X_{CO2}$ and $X_{Ar}$ denote mole fraction of $CO_2$ and Ar in the gas and $t_{CO2/Ar}$ is in °C. Note that we did not analyse $CO_2$ in the Telefon Bay bubbling gas but assumed that the gas consisted mainly of $CO_2$ (Table I). Thus, we postulate that the hydrothermal system beneath Deception Island has temperatures of ~300°C.

The temperature of the hydrothermal system has also been estimated from the chemistry of hot spring waters of the island. Chemical analyses shown in Table III indicate that the hot spring waters are mainly seawater. This is exemplified by the following enrichment factor relative to seawater, $(X/Cl)_i/(X/Cl)_{SW}$ where X denotes $Na^+$, $K^+$, $Ca^{2+}$, $Mg^{2+}$, $SO_4^{2-}$ etc., and suffixes i and SW are for sample and seawater, respectively. The enrichment factors for $Na^+$, $K^+$, $Mg^{2+}$, and $SO_4^{2-}$ range 0.7 to 1.0, suggesting a large contribution of seawater to the Deception Island hot spring waters. The $\delta^{34}S$ values of ~20‰ for $SO_4^{2-}$ measured for the hot spring waters (Table III) indicate that $SO_4^{2-}$ is mostly of seawater origin. Under such circumstances, the cation geothermometry (e.g. Na/K, $K^2$/Mg, and Na/K/Ca (Fournier 1991)) that has been widely used to estimate temperatures of water-rock interaction in hydrothermal systems could be misleading. However, Mn and $SiO_2$ in the Deception Island hot spring waters are enriched relative to seawater. Enrichment factors range from 6000 to 15 000 for Mn and from 29 to 37 for $SiO_2$. Very high Mn enrichment of hot spring waters is consistent with high Mn-Zn-Fe contents in the Port Foster sediments related to the submarine volcanic activity (Rey *et al.* 1995). The high Mn and $SiO_2$ concentrations in the hot spring waters suggest that these components are derived from water-rock interaction in the hydrothermal system. $SiO_2$ concentration in hydrothermal solution is governed by dissolution equilibrium with silica minerals. Temperature dependence of solubility of quartz, chalcedony, cristobalite and amorphous silica in water has been used as a method to estimate temperature of the water-rock interaction at depth. When applying such $SiO_2$ geothermometers, however, it is always ambiguous which silica mineral controlled the $SiO_2$ concentration of hot spring waters. For the Deception Island hot spring waters, we assumed that the waters were in equilibrium with quartz. The quartz saturation temperatures were calculated using an empirical equation proposed by Fournier & Potter (1982), i.e.

$$t_{qtz}(^{\circ}C) = -42.198 + 0.28831 \times C_{SiO2} - 3.6686 \times 10^{-4}C_{SiO2}^2 + 3.1665 \times 10^{-7} \times C_{SiO2}^3 + 77.034 \times \log(C_{SiO2}),$$

where $C_{SiO2}$ is $SiO_2$ concentration in ppm. The temperatures calculated were based on $SiO_2$ concentrations shown in Table III. They range from 146° to 160°C for hot spring waters from Fumarole Bay and Whalers Bay. If chalcedony saturation was assumed, then temperatures range from 117° to 132°C. These temperatures depend on the assumption that the sampled hot spring waters represent a liquid phase of the hydrothermal system, which has not been diluted or contaminated by groundwater or seawater during upflow to the surface, and have attained chemical equilibrium. The $SiO_2$ temperatures presented here (146°–160°C) are significantly lower than subsurface temperature of 300°C estimated using the $H_2$/Ar geothermometer for fumarolic gases. The difference suggests that the deep part of the hydrothermal system of Deception Island is overlain by cooler fluid.

The island's seismicity has been found to be most active along the major fracture zone that runs in a NE–SW direction (Fumarole Bay to Pendulum Cove) in accordance with the occurrence of areas of high geothermal activity (Ibáñez *et al.* 2000). Gaseous components of magmatic origin such as $H_2$, He and $CO_2$ migrated upward through the fractures and faults to the surface. The volcanic earthquake focal depths are shallow and are estimated to occur at 2–5 km depths. This seismicity is probably related to vaporization of the fluid by magmatic gases discharging from the magma during the latest volcanic eruptions (Correig *et al.* 1997). These shallow earthquakes occur during hydro-fracturing of crustal rocks when there is a sudden increase of volume associated with vaporization (Correig *et al.* 1997, Fournier 1999, Kusakabe *et al.* 2003).

## Hydrogen and oxygen isotopic features of waters

The hydrogen and oxygen isotopic ratios of fumarolic condensate, hot spring, crater lake and glacier meltwaters from Deception Island are listed in Table IV and graphically shown in Fig. 7. The δD and $\delta^{18}O$ values of crater lakes and glacier meltwaters range from -82 to -64 ‰ in δD and -10.9 to -7.8 ‰ in $\delta^{18}O$. They are close to meteoric waters found in mid-latitudes and reflect a close affinity of the source atmospheric water vapour to nearby oceans. Some of the surface waters appear to have been subjected to isotopic enrichment due to evaporation (DCF-15, DCW-1, DCW-5, and DCW-7 (Table IV)). Excluding these samples, the mean

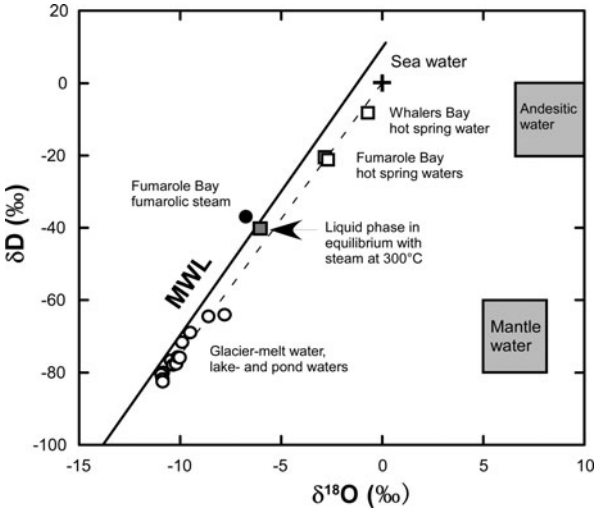


**Fig. 7.** δD and $\delta^{18}O$ relationship of thermal waters and surface waters (crater lakes, ponds and glacier meltwater) from Deception Island, Antarctica. The hot spring waters plot on a mixing line between the surface water and seawater, slightly below MWL which is a global meteoric water line defined by $\delta D = 8\delta^{18}O + 10$. Fumarolic water vapour from Fumarole Bay plot slightly above the MWL. Calculated composition of the liquid phase from which the fumarolic vapour evaporated at 300°C comes close to the hot spring water compositions. Stippled boxes indicate δD and $\delta^{18}O$ values expected for magmatic fluids from andesitic volcanoes (top) and mantle (bottom).

**Table IV.** Hydrogen and oxygen isotopic ratios of waters from Deception Island.

| Sample no. | Sample | $\delta^{18}O_{VSMOW}$ | $\delta D_{VSMOW}$ |
|---|---|---|---|
| DCF-1 | Fumarole Bay, Steam condensate, T = 98.7°C | -6.76 | -36.9 |
| DCF-7 | Fumarole Bay, Hot spring water #1, T = 53.7°C | -2.75 | -21.2 |
| DCF-20 | Fumarole Bay, Hot spring water #2, T = 50.7°C | -2.87 | -20.8 |
| DCF-16 | Whalers Bay, Hot spring water, T = 57.5°C | -0.73 | -8.3 |
| DCF-13 | Snow-meltwater flowing by Spanish Base | -10.36 | -77.9 |
| DCF-14 | Snow-meltwater flowing northern Fumarole Bay | -10.20 | -77.6 |
| DCF-15 | Snow-meltwater flowing to Whalers Bay | -9.49 | -68.7 |
| DCF-23 | Spanish Base, tap water | -10.85 | -82.5 |
| DCW-1 | Crater lake "Lago Irizar" (62°58'493"S60°42'239"W) | -8.61 | -64.2 |
| DCW-2 | Crater lake "Soto Crater" (62°59'05.2"S, 60°39'16.9"W) | -10.51 | -76.7 |
| DCW-3 | Crater lake, name unknown (62°58'57.6"S, 60°40.01.1 "W) | -10.04 | -75.9 |
| DCW-4 | Crater lake "Crater Zapatilla (Shoes Lake)" (62°58'59.3"S, 60°40.35.9"W) | -10.89 | -80.9 |
| DCW-5 | Pond, name unknown (62°55'29.1"S, 60°40'56.7"W) | -7.79 | -63.9 |
| DCW-6 | Crater Lake, name unknown (62°55'26.1 "S, 60°40'52.2"W) | -10.86 | -81.9 |
| DCW-7 | Pond, name unknown (62°58'51.5"S, 60°39'55.5"W) | -9.87 | -71.5 |
| DCW-8 | Rio Mecon (MeKong River) (62°58'37.7"S, 60°40'39.2"W) | -10.77 | -80.0 |
| DCW-9 | Crater lake "Chacao Crater" (62°56'00.0"S, 60°40'55.7"W) | -10.01 | -76.0 |

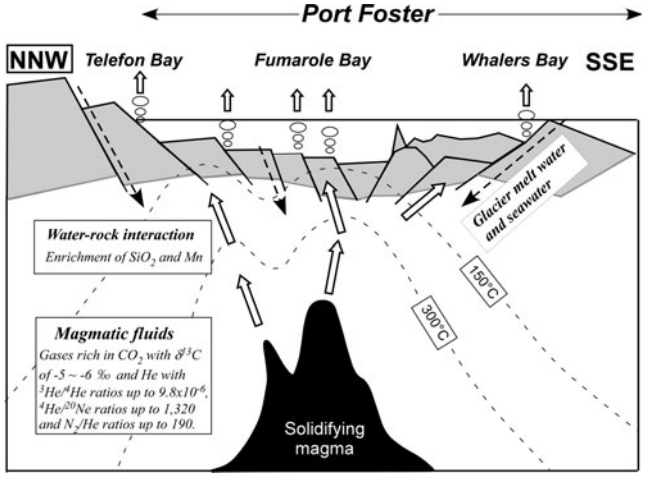


**Fig. 8.** Schematic representation of the hydrothermal system beneath Deception Island along the NNW–SSE cross section (modified from Somoza *et al.* 2004). Magmatic He and $CO_2$ carrying the isotopic signatures of the source mantle beneath the Bransfield basin come from the solidifying magma and reach the surface through the faults and fractures. The hydrothermal system develops widely beneath the island. The temperature of deep part of the system is around 300°C and that of overlying shallow part is *c.* 150°C as shown by dashed curves. Fumarole Bay where the fumarolic activity is currently highest is off the cross section and is located at the western end of Port Foster (Fig. 1).

δD and $\delta^{18}O$ values of local meteoric waters are -78.8 ‰ in δD and -10.50 ‰ in $\delta^{18}O$. The hot spring waters plot on a mixing line between seawater and the local meteoric water. The mixing line is slightly below the global meteoric water line (MWL; $\delta D = 8\delta^{18}O + 10$). The hot spring waters were collected near the seashore, so that they were greatly influenced by seawater as shown in Fig. 7. The seawater contribution to the hot spring waters is 0.73 for the Fumarole Bay samples (DCF-7 and DCF-20) and 0.93 for the Whalers Bay sample (DCF-16). Water vapour in the Fumarole Bay fumarolic gas (DCF-1) may represent steam evaporated from the deep hydrothermal fluid of the island. The δD and $\delta^{18}O$ values of the liquid may be calculated assuming a single step equilibrium evaporation at 300°C, which is the temperature estimated from the $H_2$/Ar geothermometer. The calculation was done using an equation for isotopic fractionation between liquid and vapour phases, i.e. $\alpha = (1 + \delta^{18}O_{liq}/1000)/ (1 + \delta^{18}O_{vap}/1000)$ in the case of oxygen isotopes, where α is an oxygen isotopic fractionation factor at a given temperature. Hydrogen and oxygen isotopic fractionation factors between vapour and liquid of water including the salinity effect were taken from Horita *et al.* (1993). The calculated δD and $\delta^{18}O$ values are -40‰ and -6.0‰, respectively, and are plotted as a solid square in Fig. 7. The square lies close to the mixing line between seawater and local meteoric water and indicates a seawater fraction of approximately 0.43. A magmatic contribution cannot be detected from the δD and $\delta^{18}O$ signatures (Fig. 7). However, helium in fumarolic, bubbling and hot spring gases was carried to the surface by magmatic $CO_2$. The helium was not contaminated significantly by atmospheric helium dissolved in surface water and seawater, because it is enriched by a factor of up to 1000 relative to air (Fig. 4).

## Conclusions

The $^3He/^4He$ ratios of $9.4 \sim 9.8 \times 10^{-6}$ and the $\delta^{13}C$ values of -5 to around -6‰ for fumarolic gases, bubbling gases, and hot spring waters from Deception Island, Antarctica, suggest that He and $CO_2$ are of mantle origin. The magma emplaced beneath the island was derived from the wedge mantle that was geochemically similar to MORB source mantle. But this mantle was contaminated by U, Th, Sr and Pb derived from a slab that had previously subducted beneath the Bransfield Basin back-arc basin. This interpretation is supported by the observed $^3He/^4He$ ratios that are slightly lower than the MORB values and the $N_2$/He ratios of the gases that are higher than those of MORB-derived basaltic gases. Figure 8 illustrates a schematic view of the hydrothermal system. The subsurface temperature of deep part of the hydrothermal system is around 300ºC as indicated by the $H_2$/Ar gas geothermometer. Gaseous components such as He and $CO_2$ came from the underlying magma, moved through the fractures and faults without contamination by atmospheric components dissolved in groundwater and seawater, and reached the surface as a gas phase. Hot spring waters represent the shallow part of the hydrothermal system with temperatures around 150ºC as estimated by the $SiO_2$ geothermometer. The major dissolved ionic components and $\delta D$-$\delta^{18}O$-$\delta^{34}S$ values indicated that the hot spring waters were mixed with a large proportion of seawater.

## Acknowledgements

This study was supported by the KOPRI projects PE08020 and PP08030. We thank Mr Rafael Ayora Hirsh, commander of the Spanish Antarctic Base at Deception Island, and his team for their kind logistic support. The manuscript was prepared while MK was working for Univ. Toyama, Japan. We thank L. Somoza and D.R. Hilton for their critical review on the earlier version of the manuscript. English was improved by G.L. Scott.

## References

Aka, F.T., Kusakabe, M., Nagao, K. & Tanyileke, G.T. 2001. Noble gas isotopic compositions and water/gas chemistry of soda springs from the islands of Bioko, Sao Tome and Annobon, along with Cameroon Volcanic Line, West Africa. *Applied Geochemistry*, **16**, 323–338.

Ballentine, C.J. & Burnard, P.G. 2002. Production, release and transport of noble gases in continental crust. *In* Porcelli, D., Ballentine, C.J. & Wieler, R., *eds. Noble gases in geochemistry and cosmochemistry. Reviews in Mineralogy and Geochemistry*, **47**, 481–537.

Ballentine, C.J., Burgess, R. & Marty, B. 2002. Tracing fluid origin, transport and interaction in the crust. *In* Porcelli, D., Ballentine, C.J. & Wieler, R., *eds. Noble gases in geochemistry and cosmochemistry. Reviews in Mineralogy and Geochemistry*, **47**, 539–614.

Chako, T., Cole, D.R. & Horita, J. 2001. Equilibrium oxygen, hydrogen and carbon isotope fractionation factors applied to geologic systems. *In* Valley, J.W. & Cole, D.R., *eds. Stable isotope geochemistry. Reviews in Mineralogy and Geochemistry*, **431**, 1–81.

Choe, W.H., Lee, J.I., Lee, M.J., Hur, S.D. & Jin, Y.K. 2007. Origin of E-MORB in a fossil spreading center: the Antarctic–Phoenix Ridge, Drake Passage, Antarctica. *Geoscience Journal*, **11**, 185–199.

Correig, A.M., Urquizu, M., Vila, J. & Marti, J. 1997. Analysis of the temporal occurrence of seismicity at Deception Island (Antarctica): a nonlinear approach. *Pure and Applied Geophysics*, **149**, 553–574.

Lide, D.R. *CRC Handbook of Chemistry and Physics*, 74th ed. Boca Raton, FL: CRC Press.

Fournier, R.O. 1991. Water geothermometers applied to geothermal energy. *In* D'Amore, F. *ed. Application of geochemistry in geothermal reservoir development*. Rome: UNITAR/UNDP Centre for Small Energy Resources, 37–69.

Fournier, R.O. 1999. Hydrothermal processes related to movement of fluid from plastic into brittle rock in the magmatic-epithermal environment. *Economic Geology*, **94**, 1193–1211.

Fournier, R.O. & Potter II, R.W. 1982. An equation correlating the solubility of quartz in water from 25°C to 900°C at pressures up to 10,000 bars. *Geochimica et Cosmochimica Acta*, **46**, 1969–1974.

Fretzdorff, S., Worthington, T.J., Haase, K.M., Hekinian, R., Franz, L., Keller, R.A. & Stoffers, P. 2004. Magmatism in the Bransfield Basin: Rifting of the South Shetland Arc? *Journal of Geophysical Research*, **109**, 10.1029/2004JB003046.

Fukumoto, H., Nagao, K. & Matsuda, J. 1986. Noble gas studies on the host phase of high $^{3}He/^{4}He$ ratios in deep-sea sediments. *Geochimica et Cosmochimica Acta*, **50**, 2245–2253.

Giggenbach, W.F. 1987. Redox processes governing the chemistry of fumarolic gas discharges from White Island, New Zealand. *Applied Geochemistry*, **2**, 143–161.

Giggenbach, W.F. 1991. Chemical techniques in geothermal exploration. *In* D'Amore, F., *ed. Application of geochemistry in geothermal reservoir development*. Rome: UNITAR/UNDP Centre for Small Energy Resources, 119–144.

Giggenbach, W.F. 1997. The origin and evolution of fluids in magmatic-hydrothermal systems. *In* Barnes, H.L., *ed. Geochemistry of Hydrothermal Ore Deposits*, 3rd ed. New York: John Wiley, 737–796.

Graham, D.W. 2002. Noble gas isotope geochemistry of mid-ocean ridge and ocean island basalts: characterization of mantle source reservoirs. *In* Porcelli, D., Ballentine, C.J. & Wieler, R., *eds. Noble gases in geochemistry and cosmochemistry. Reviews in Mineralogy and Geochemistry*, **47**, 247–317.

Hilton, D.R., Fischer, T.P. & Marty, B. 2002. Noble gases and volatile recycling at subduction zones. *In* Porcelli, D., Ballentine, C.J. & Wieler, R., *eds. Noble gases in geochemistry and cosmochemistry. Reviews in Mineralogy and Geochemistry*, **47**, 319–370.

Hilton, D.R., Hammerschmidt, K., Loock, G. & Friedrichsen, H. 1993. Helium and argon isotope systematics of the central Lau Basin and Valu Fa Ridge: evidence of crust/mantle interactions in a back-arc basin. *Geochimica et Cosmochimica Acta*, **57**, 2819–2841.

Horita, J., Cole, D.R. & Wesolowski, D.J. 1993. The activity-composition relationship of oxygen and hydrogen isotopes in aqueous salt solutions: III. Vapor-liquid water equilibration of NaCl solutions to 350°C. *Geochimica et Cosmochimica Acta*, **59**, 1139–1151.

Ibáñez, J.M., Del Pezzo, E., Almendros, J., La Rocca, M., Alguacil, G., Ortiz, R. & Garcia, A. 2000. Seismovolcanic signals at Deception Island volcano, Antarctica: wave field analysis and source modelling. *Journal of Geophysical Research*, **105**, 13 905–13 931.

Ishibashi, J., Sano, Y., Wakita, H., Gamo, T., Tsutsumi, M. & Sakai, H. 1995. Helium and carbon geochemistry of hydrothermal fluids from the Mid-Okinawa Trough back arc basin, southeast of Japan. *Chemical Geology*, **123**, 1–15.

Keller, R.A., Fisk, M.R., Smellie, J.L., Strelin, J.A., Lawver, L.A. & White, W.M. 2002. Geochemistry of back-arc basin volcanism in Bransfield Strait, Antarctica: subducted contributions and along-axis variations. *Journal of Geophysical Research*, **107**, 10.1029/2001JB000444.

Kipfer, R., Aeschbah-Hertig, W., Peeters, F. & Stute, M. 2002. Noble gases in lakes and ground waters. *In* Porcelli, D., Ballentine, C.J. & Wieler, R., *eds. Noble gases in geochemistry and cosmochemistry. Reviews in Mineralogy and Geochemistry*, **47**, 615–700.

Kita, I., Nitta, K., Nagao, K., Taguchi, S. & Koga, A. 1993. Difference in $N_2/Ar$ ratio of magmatic gases from northeast and southwest Japan: new evidence for different states of plate subduction. *Geology*, **21**, 391–394.

Klinkhammer, G.P., Chin, C.S., Keller, R.A., Dahlmann, A., Sahling, H., Sarthou, G., Petersen, S., Smith, F. & Wilson, C. 2001. Discovery of new hydrothermal vent sites in Bransfield Strait, Antarctica. *Earth and Planetary Science Letters*, **193**, 395–407.

Kraus, S. 2005. *Magmatic dyke systems of the South Shetland Islands volcanic arc* (*West Antarctica*)*: reflections of the geodynamic history*. PhD thesis, University of Munich, 160 pp. (available online at http://edoc.ub.uni-muenchen.de/archive/00003827/).

Kusakabe, M., Ohwada, M., Satake, H., Nagao, K. & Kawasaki, I. 2003. Helium isotope ratios and geochemistry of volcanic fluids from the Norikura Volcanic chain, central Japan: implications for crustal structures and seismicity. *Society of Economic Geologists Special Publication*, **10**, 75–89.

Lee, M.J., Lee, J.I., Choe, W.H. & Park, C.-H. 2008. Trace element and isotopic evidence for temporal changes of the mantle sources in the South Shetland Islands, Antarctica. *Geochemical Journal*, **42**, 207–219.

Macpherson, C.G., Hilton, D.R., Sinton, J.M., Poreda, R.J. & Craig, H. 1998. High $^{3}He/^{4}He$ ratios in the Manus backarc basin: implications for mantle mixing and the origin of plumes in the western Pacific Ocean. *Geology*, **26**, 1007–1010.

Maestro, A., Somoza, L., Rey, J., Martinez-Frias, J. & Lopez-Martinez, J. 2007. Active tectonics, fault patterns, and stress field of Deception Island: a response to oblique convergence between the Pacific and Antarctic plates. *Journal of South American Earth Sciences*, **23**, 256–268.

Marty, B. & Jambon, A. 1987. $C/^{3}He$ in volatile fluxes from the solid Earth: implications for carbon geodynamics. *Earth and Planetary Science Letters*, **83**, 16–26.

Matsuo, S., Suzuki, M. & Mizutani, Y. 1978. Nitrogen to argon ratio in volcanic gases. *Advances in Earth and Planetary Sciences*, **3**, 17–25.

Nishio, Y., Sasaki, S., Gamo, T., Hiyagon, H. & Sano, Y. 1998. Carbon and helium isotope systematics of North Fiji Basin basalt glasses: carbon geochemical cycle in the subduction zone. *Earth and Planetary Science Letters*, **154**, 127–138.

Orsi, A.H. & Whitworth III, T. 2005. *Hydrographic Atlas of the World Ocean Circulation Experiment* (WOCE). Vol. 1: Southern Ocean. College Station, TX: Texas A&M University.

Ortiz, R., Valentin, A. & Grimalt, J. 1987. Actividad fumaroliana en Decepcion. *Estudio preliminary. II Symposio Espanol de Estudios Antarticos*. Madrid: CSIC, 229–237. [Not seen].

Ozima, M. & Alexander, Jr E.C. 1976. Rare gas fractionation patterns in terrestrial samples and the earth-atmosphere evolution model. *Reviews of Geophysics and Space Physics*, **14**, 385–390.

Ozima, M. & Podosek, F.A. 2002. *Noble gas geochemistry*. Cambridge: Cambridge University Press, 286 pp.

Park, M., Dziak, R.P., Matsumoto, H., Bohnenstiehl, D.R., Haxel, J.H. & Lee, W.S. 2007. Hydroacoustic monitoring of the Bransfield Strait and Drake Passage, Antarctica: a first analysis of seafloor seismicity and cryogenic acoustic sources. *Proceedings 14th KOPRI international symposium on polar sciences: Polar Regions in Global Change*. Songdo Techno Park, Incheon, Korea, 42–47.

Pearce, J.A., Baker, P.E., Harvey, P.K. & Luff, I.W. 1995. Geochemical evidence for subduction fluxes, mantle melting and fractional crystallization beneath the South Sandwich island arc. *Journal of Petrology*, **36**, 1073–1109.

Poreda, R.J. & Craig, H. 1992. He and Sr isotopes in the Lau basin mantle - depleted and primitive mantle components. *Earth and Planetary Science Letters*, **113**, 487–493.

Rey, J., Somoza, L. & Martínez-Frías, J. 1995. Tectonic, volcanic, and hydrothermal event sequence on Deception Island (Antarctica). *Geo-Marine Letters*, **15**, 1–8.

Sano, Y. & Marty, B. 1995. Origin of carbon in fumarolic gas from island arcs. *Chemical Geology*, **119**, 265–274.

Schlosser, P., Suess, E., Bayer, R. & Rhein, M. 1988. $^{3}$He in the Bransfield Strait waters: indication of local injection from back-arc rifting. *Deep-Sea Research*, **35**, 1919–1935.

Shaw, A.M., Hilton, D.R., Macpherson, C.G. & Sinton, J.M. 2004. The C-He-Ar systematics of lavas from the Manus back-arc basin: resolving degassing and contamination. *Geochimica et Cosmochimica Acta*, **68**, 1837–1856.

Smellie, J.L. 2001. Lithostratigraphy and volcanic evolution of Deception Island, South Shetland Islands. *Antarctic Science*, **13**, 188–209.

Smellie, J.L. & López-Martínez, J. 2000. *Geological map of Deception Island. BAS GEOMAP Series, Sheet 6A, 1:25000*. Cambridge: British Antarctic Survey.

Somoza, L., Martinez-Frias, J., Smellie, J.L., Rey, J. & Maestro, A. 2004. Evidence for hydrothermal venting and sediment volcanism discharged after recent short-lived volcanic eruptions at Deception Island, Bransfield Strait, Antarctica. *Marine Geology*, **203**, 119–140.

Taran, Y.A. 1986. Gas geothermometers for hydrothermal systems. *Geochemistry International*, **23**, 111–126.

Taylor, B.E. 1986. Magmatic volatiles: isotopic variation of C, H, and S. *Reviews in Mineralogy*, **16**, 185–225.

Torgersen, T. & Jenkins, W.J. 1982. Helium isotopes in geothermal systems: Iceland, the Geysers, Raft River and Steamboat Springs. *Geochimica et Cosmochimica Acta*, **46**, 739–748.

Valentin, A., Martini, M. & Diez-Gil, J.L. 1989. Geoquimica de fluidos en Isla Decepcion. *Final Proceedings III Symposio Espanol Estudios Antarticos, Gredos*, 195–202.[Not seen].

van Soest, M.C., Hilton, D.R. & Kreulen, R. 1998. Tracing crustal and slab contributions to arc magmatism in the Lesser Antilles island arc using helium and carbon relationships in geothermal fluids. *Geochimica et Cosmochimica Acta*, **62**, 3323–3335.